Pol. J. Environ. Stud. Vol. XX, No. X (XXXX), 1-14
DOI: *10.15244/pjoes/220229* ONLINE PUBLICATION DATE: 2026-07-30

Original Research

Study on Low-Temperature Methanation of Coal Pyrolysis Gas over Ni-Based Catalysts with Core-Shell Structure

Jihao Chen[1, 2]*, Pengjie Miao[1, 2], Ye Li[1, 2], Qin Guo[1, 2], Wenbo Zhao[1, 2], Song Junli[1, 2]**

[1]College of Energy and Chemical Engineering, Xinjiang Institute of Technology, Aksu 843100, China
[2]Xinjiang Key Laboratory of New Energy and Energy Storage Technology, Xinjiang Institute of Technology, Aksu 843100, China

Received: 13 November 2025
Accepted: 31 March 2026

Abstract

In this study, a series of SiO_2@ZrO_2-supported catalysts was employed for the methanation of CO/CO_2 in a fixed-bed reactor to address the issues of insufficient low-temperature activity and sulfur poisoning of catalysts during CO/CO_2 methanation. Mesoporous SiO_2@ZrO_2 core–shell supports were prepared via the sol-gel method and liquid-phase coating process, and Ni-CeO_2-ZnO catalysts supported on SiO_2@ZrO_2 were synthesized by incipient wetness impregnation with Ni as the active component and CeO_2-ZnO as promoters. Catalysts with optimal methanation performance and sulfur resistance were screened by regulating the ZrO_2 shell loading (7%, 15%, 23%), Ni loading (5%, 10%, 15%, 20%), and Ce/Zn promoter molar ratio (3:1, 1:1, 1:3). The structural properties and catalytic mechanism were analyzed using multiple characterization techniques, including XRD, SEM, TEM, XPS, and H2-TPR. The results showed that: (1) the Ni-CeO_2-ZnO/SiO_2@ZrO_2 catalyst achieved CO and CO_2 conversions of 92.37% and 87.63%, respectively, with CH4 selectivity exceeding 99%; after exposure to 50 ppm H_2S, the catalyst retained 85% of its initial activity in a 500 h stability test. (2) Characterization revealed that the mesoporous SiO_2@ZrO_2 support suppressed Ni sintering and accelerated mass transfer; ZnO preferentially adsorbed H_2S to form ZnS, protecting the Ni active sites, thereby enabling efficient CO/CO_2 methanation and sulfur resistance of the catalyst.

Keywords: mesoporous, core-shell, CeO_2-ZnO, Ni, methanation, sulfur resistance

Introduction

Under the global background of advancing carbon peaking and carbon neutrality, carbon reduction is a core issue in energy structure transformation and industrial green development [1]. As a basic energy source, coal remains irreplaceable in the short term, making its low-carbon utilization crucial. Coal pyrolysis, a core technology for coal graded conversion, produces mixed gas rich in CO, CO_2, H_2, and light hydrocarbons. Upgrading this gas to synthetic natural gas (SNG) via methanation alleviates the contradiction between natural

*e-mail: 1506758427@qq.com
**e-mail: 17799530161@163.com
0000-0002-8497-5635

gas supply and demand, realizes clean coal-based energy utilization [2], fixes greenhouse gases to reduce emissions, and allows SNG to be widely used due to its advantages. Efficient methanation of coal pyrolysis gas is an important bridge connecting coal resources and clean energy demand [3], with great practical and strategic value for the low-carbon transformation of the coal industry and energy security.

However, the methanation of coal pyrolysis gas faces two core technical bottlenecks that severely restrict its industrial application. On the one hand, the high CO (20%-40%) and CO_2 (10%-20%) contents are hard to convert efficiently at low temperatures [4]. Traditional Ni/Al_2O_3 catalysts demand temperatures above 400ºC for a high conversion [5], which raises energy consumption, accelerates equipment corrosion, and leads to catalyst loss. On the other hand, trace sulfur (e.g., 50-500 ppm H_2S) strongly binds to active metals, forming stable sulfides and causing permanent deactivation [6]. High temperatures also induce metal sintering and carbon deposition [7], shortening catalyst lifetime and raising operational costs. The solution lies in catalyst design and optimization. Developing catalysts with high low-temperature activity, strong sulfur resistance, and good anti-sintering and anti-carbon deposition properties is key to advancing this technology from lab to industrial application.

Currently, research on methanation catalysts for coal pyrolysis gas has made certain progress. Researchers mainly optimize catalyst performance through three directions: support selection, active component regulation, and promoter modification [8], but existing schemes still have obvious limitations. In terms of active components, nickel-based catalysts have become the mainstream research choice due to their low cost and high methanation activity [9]. However, their sole use suffers from problems such as poor dispersion of active components, susceptibility to sulfur poisoning, and easy sintering at high temperatures. Precious metal (e.g., Ru, Rh) catalysts exhibit higher low-temperature activity and sulfur resistance [10], but their high cost limits large-scale industrial application. In terms of support selection, traditional supports such as Al_2O_3, SiO_2, and ZrO_2 each have advantages and disadvantages. Al_2O_3 has a moderate interaction with Ni, which can improve the dispersion of active components, but it easily forms a stable $NiAl_2O_4$ spinel structure with Ni at high temperatures, leading to decreased activity [11]. SiO_2 possesses a high specific surface area and mesoporous structure, which is beneficial for mass transfer and active component loading, but its weak interaction with Ni fails to effectively inhibit Ni particle sintering [12]. ZrO_2, relying on strong metal-support interaction and abundant oxygen vacancies, can significantly enhance the catalyst's sintering resistance and CO_2 adsorption-activation capacity. However, its low specific surface area results in high mass transfer resistance, making it difficult to adapt to the rapid conversion of high-concentration CO/CO_2 [13]. In terms of promoter modification, CeO_2 has excellent oxygen storage and release capabilities due to the redox cycling property of Ce^{3+}/Ce^{4+} [14]. It can promote carbon deposition oxidation and CO/CO_2 activation, effectively alleviating carbon deposition issues. ZnO modulates the adsorption energy of Ni active sites through electronic effects [15], and simultaneously has a certain adsorption capacity for H_2S, which can reduce the impact of sulfur poisoning. Nevertheless, a single promoter cannot solve the three major problems of sulfur poisoning, sintering, and carbon deposition simultaneously. Moreover, the synergistic effects among supports, active components, and promoters have not been fully explored. Therefore, existing catalyst designs struggle to balance low-temperature activity, stability, and sulfur resistance. An innovative catalyst structure design is urgently needed to integrate the advantages of different materials and achieve the synergistic regulation of the support, active component, and promoter.

The emergence of core-shell structured supports provides a new approach to addressing the aforementioned issues. By compositing two or more materials in a "core-shell" configuration, core-shell structures can integrate the advantages of different components at the microscale. Using a material with a high specific surface area as the core ensures the catalyst's mass transfer efficiency and active component loading capacity. Using a functional material as the shell can regulate the electronic state and dispersion of active components through strong interactions, while endowing the catalyst with properties such as sulfur resistance and sintering resistance. In the field of methanation catalysts, the design of $SiO_2@ZrO_2$ core-shell supports exhibits unique advantages [16]. With mesoporous SiO_2 as the core, its high specific surface area and ordered mesoporous structure are retained, which significantly reduces mass transfer resistance and adapts to the rapid diffusion of high-concentration components in coal pyrolysis gas. With ZrO_2 as the shell, the strong metal-support interaction can stabilize Ni active components and inhibit particle sintering. Meanwhile, the Lewis acid sites and oxygen vacancies on the ZrO_2 surface can enhance the adsorption and activation capacity of CO_2. Furthermore, introducing CeO_2 and ZnO as composite promoters can further exert their synergistic effect. The redox cycle of CeO_2 provides oxygen vacancies and promotes carbon deposition oxidation. The sulfur adsorption capacity of ZnO enables it to react preferentially with H_2S, protecting Ni active sites. The combination of the two can solve the problems of carbon deposition and sulfur poisoning simultaneously. However, current research on Ni-supported mesoporous $SiO_2@ZrO_2$ core-shell supports with CeO_2-ZnO composite promoters has not yet been reported. Their mechanism of action in the low-temperature methanation of high-concentration CO/CO_2 in coal pyrolysis gas, as well as the synergistic effect among support, active component, and promoters, remains unclear. This research gap provides room for the design of innovative catalysts.

Based on the aforementioned research status and technical requirements, this study proposes, for the first time, a catalyst design strategy that combines a mesoporous SiO_2@ZrO_2 core-shell structure, CeO_2-ZnO composite promoters, and Ni active components. Firstly, the SiO_2@ZrO_2 core-shell support is constructed: the high specific surface area and mesoporous structure of the SiO_2 core enhance mass transfer efficiency, while the strong metal-support interaction of the ZrO_2 shell improves the dispersion and stability of Ni active components. This addresses the issue that traditional supports cannot simultaneously achieve a high specific surface area and strong interaction. Secondly, CeO_2-ZnO composite promoters are introduced: the carbon deposition resistance of CeO_2 and the sulfur resistance of ZnO are utilized to achieve dual enhancement of "sulfur resistance-carbon deposition resistance", making up for the limitation of a single functionality in a single promoter. The final prepared catalyst achieves systematic optimization of support structure, active component loading, and promoter ratio, breaking through the bottlenecks of traditional catalysts such as insufficient low-temperature activity, poor sulfur resistance, and low stability.

Materials and Methods

Experimental Materials and Reagents

All chemical reagents used in this experiment are of analytical grade and used directly without further purification, as specified below:

Silicon source: Tetraethyl orthosilicate (TEOS, purity≥99%, Sinopharm Chemical Reagent Co., Ltd.); Zirconium source: Zirconium oxychloride octahydrate ($ZrOCl_2 \cdot 8H_2O$, purity≥99%, Aladdin Reagent Co., Ltd.); Metal salt precursors: Nickel nitrate hexahydrate ($Ni(NO_3)_2 \cdot 6H_2O$, purity≥98%), Cerium nitrate hexahydrate ($Ce(NO_3)_3 \cdot 6H_2O$, purity≥99%), Zinc nitrate hexahydrate ($Zn(NO_3)_2 \cdot 6H_2O$, purity≥98%), all purchased from Sinopharm Chemical Reagent Co., Ltd.

Template and solvent: Triblock copolymer P123 ($EO_{20}PO_{70}EO_{20}$, average molecular weight 5800, Sigma-Aldrich), Anhydrous ethanol (C_2H_5OH, purity≥99.7%), Ammonia water ($NH_3 \cdot H_2O$, mass fraction 25%-28%), all purchased from Sinopharm Chemical Reagent Co., Ltd.

Gases: Hydrogen (H_2, purity 99.99%), Nitrogen (N_2, purity 99.99%), Argon (Ar, purity 99.99%), Simulated coal pyrolysis gas (volume composition: CO_2 10%, CO 12%, H_2 76%, N_2 2%), Hydrogen sulfide (H_2S, purity 99.9%, the balance gas is N_2), all provided by Nanjing Special Gas Factory.

Catalyst Preparation

Synthesis of Mesoporous SiO_2 Core

The mesoporous SiO_2 core is prepared by the sol-gel method combined with template removal. 2 g of P123 is dissolved in a mixed solution of 80 mL anhydrous ethanol and 40 mL deionized water and magnetically stirred at 30ºC for 30 min until completely dissolved. 10 mL of TEOS is slowly added dropwise, and after continuous stirring for 10 minutes, ammonia water is used to adjust the pH of the solution to 8.5. The mixture is stirred at a constant temperature of 30ºC for 24 h to form a white gel. The gel is transferred to a polytetrafluoroethylene hydrothermal kettle, subjected to hydrothermal reaction at 80ºC for 24 h, cooled, filtered, alternately washed with deionized water and ethanol 3 times, and vacuum-dried at 60ºC for 12 h. The dried sample is placed in a muffle furnace, heated to 550ºC at a rate of 2ºC/min, and calcined in an air atmosphere for 6 h (to remove the P123 template), resulting in a mesoporous SiO_2 core, denoted as m-SiO_2.

Synthesis of Mesoporous SiO_2@ZrO_2 Core-Shell Support

The core-shell support is prepared by a liquid-phase coating method, with the ZrO_2 shell loading regulated. 1g of m-SiO_2 is weighed and dispersed in 100 mL of anhydrous ethanol, followed by ultrasonic treatment for 30 min to form a uniform suspension. The amount of $ZrOCl_2 \cdot 8H_2O$ required is calculated according to the target ZrO_2 shell loadings (7%, 15%, 23%). The $ZrOCl_2 \cdot 8H_2O$ is dissolved in 20 mL of deionized water and added dropwise to the above suspension. Ammonia water is used to adjust the pH of the mixture to 9.0, and the mixture is magnetically stirred at 50ºC for 4 h to allow Zr^{4+} to hydrolyze on the surface of m-SiO_2 and form a ZrO_2 precursor. After filtration and washing, the product is vacuum-dried at 60ºC for 12 h, then heated to 500ºC at a rate of 2ºC/min in a muffle furnace and calcined in an air atmosphere for 4 h. Core-shell supports with different ZrO_2 shell thicknesses are obtained, denoted as m-SiO_2@ZrO_2-t (where t is the ZrO_2 shell loading).

Preparation of Ni-CeO_2-ZnO/m-SiO_2@ZrO_2 Catalyst

The active components and promoters are loaded by the incipient wetness impregnation method. $Ni(NO_3)_2 \cdot 6H_2O$, $Ce(NO_3)_3 \cdot 6H_2O$, and $Zn(NO_3)_2 \cdot 6H_2O$ are weighed according to the target loadings (Ni: 5%-20%; total loading of CeO_2 and ZnO: 10% based on the mass of the support) and dissolved in deionized water to prepare a mixed impregnating solution. The m-SiO_2@ZrO_2 support is mixed with the impregnating solution, left to stand at room temperature for 12 h, then vacuum-dried at 60ºC for 12 h. Subsequently, the sample is

heated to 500ºC at a rate of 2°C/min in a muffle furnace and calcined in an air atmosphere for 4 h to obtain the catalyst precursor. The precursor is placed in a quartz tube reactor and reduced at 400ºC for 3 h (heating rate: 5ºC/min) in a H_2/Ar mixed gas flow (volume ratio 1:9, flow rate 50 mL/min). After naturally cooling to room temperature, the gas is switched to Ar for protection, yielding the reduced catalyst. A series of catalysts is prepared by adjusting the Ni loading (5%, 10%, 15%, 20%), Ce/Zn molar ratio (3:1, 1:1, 1:3), and support type, denoted as Ni_x-$Ce_yZn_{1-y}O$/m-SiO_2@ZrO_2-t (where x is the Ni loading, y is the molar ratio of Ce in Ce+Zn, and t is the ZrO_2 shell loading).

Catalyst Performance Evaluation

Activity and Selectivity Evaluation

Fig. 1 shows the flow chart of the methanation performance test. The coal pyrolysis gas methanation performance test is carried out in a fixed-bed quartz reactor (inner diameter 8 mm). The catalyst loading is 0.2 g (40-60 mesh), and quartz sand (40-60 mesh) is filled above and below to eliminate dead volume. Before the reaction, the catalyst is in-situ reduced at 400ºC for 3 h in a H_2/Ar (volume ratio 1:9) gas flow (50 mL/min), and then cooled to the reaction temperature of 250-300ºC. Simulated coal pyrolysis gas is introduced, with a composition of 12% CO, 10% CO_2, 76% H_2, and 2% N_2, at a flow rate of 100 mL/min, and the reaction is carried out under normal pressure. Samples are taken for analysis after the reaction stabilizes for 2 h; the products are detected online by a gas chromatograph GC-2014: a TCD detector is used to analyze CO, CO_2, H_2, and N_2; a FID detector is used to analyze CH_4 and C^{2+} hydrocarbons.

The calculation formulas for conversion rate and selectivity are as follows:

CO conversion rate: $X_{CO} = \frac{n_{CO,\ in} - n_{CO,\ out}}{n} \times 100\%$;

CO_2 conversion rate: $X_{CO_2} = \frac{n_{CO_2,\ in} - n_{CO_2,\ out}}{n_{CO_2,\ in}} \times 100\%$;

CH_4 selectivity: $S_{CH_4} = \frac{n_{CH_4,\ out}}{(n_{CO,\ in} - n_{CO,\ out}) + (n_{CO_2,\ in} - n_{CO_2,\ out})} \times 100\%$.

Evaluation of Stability and Sulfur Resistance

Stability test: At the optimal activity temperature, simulated coal pyrolysis gas is continuously introduced, and the operation lasts for 500 h. Samples are taken for analysis every 10 h to record changes in CO/CO_2 conversion rates and CH_4 selectivity.

Sulfur resistance test: H_2S with a concentration of 50 ppm is introduced into the simulated coal pyrolysis gas, and the reaction is carried out at the optimal temperature for 500 h to monitor changes in activity. Then, H_2S with a concentration of 500 ppm is introduced; after maintaining stability for a certain period, the supply of H_2S is stopped to investigate the activity recovery ability.

Catalyst Characterization

(1) X-ray diffraction (XRD): A Bruker D8 Advance diffractometer (Cu Kα radiation, λ = 0.15418 nm) is used, with a scanning range of 2θ = 10°-80°, step size of 0.02°, tube voltage of 40 kV, and tube current of 40 mA. It is employed to analyze the phase composition and crystallite size (using the Scherrer formula: d = Kλ/(βcosθ), K=0.89).

(2) Scanning electron microscopy (SEM): Scanning electron microscopy can obtain the surface characteristics of catalyst samples. In this study, the SEM model is JSM-6460LV (manufactured by JEOL Ltd.) with an operating voltage of 20 kV.

(3) Transmission electron microscopy (TEM): A FEI Talos F200X transmission electron microscope is used at an accelerating voltage of 200 kV to observe the core-shell structure and dispersion of active components.

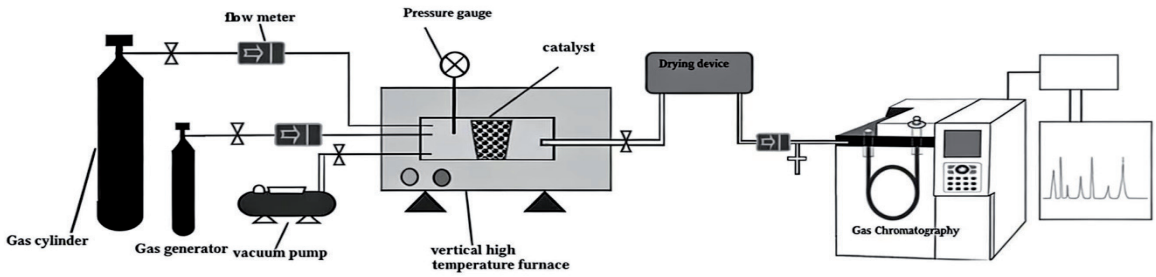

Fig. 1. Flow chart of methanation performance test process.

(4) N_2 adsorption-desorption (BET): A Micromeritics ASAP 2460 physical adsorption instrument is utilized. Samples are first degassed under vacuum at 200ºC for 6 h. The specific surface area is calculated using the Brunauer-Emmett-Teller (BET) method, and the pore size distribution is analyzed by the Barrett-Joyner-Halenda (BJH) method.

(5) X-ray photoelectron spectroscopy (XPS): A Thermo Scientific ESCALAB 250Xi photoelectron spectrometer (Al Kα radiation, hν = 1486.6 eV) is used. The binding energy is calibrated with C 1s (284.8 eV) as the internal standard to analyze the surface element valence states and chemical environments.

(6) H_2 temperature-programmed reduction (H_2-TPR): A Micromeritics AutoChem II 2920 chemisorption instrument is employed. The sample (50 mg) is pretreated in an Ar flow (50 mL/min) at 300ºC for 1 h, cooled to 50ºC, then switched to a 10% H_2/Ar mixture (50 mL/min), and heated to 800ºC at a rate of 10ºC/min. The H_2 consumption signal is detected by TCD.

Results and Discussion

Performance Evaluation and Characterization Analysis of Mesoporous SiO_2@ZrO_2 Core-Shell Support

Effect of ZrO_2 Shell Loading on Pyrolysis Gas Methanation

Fig. 2 shows the effects of m-SiO_2@ZrO_2 core-shell supports with ZrO_2 shell loadings of 7%, 15%, and 23% on CO/CO_2 conversion rates and CH_4 selectivity, with the activity evaluation temperature being 300ºC. It can be seen from the figure that the CO/CO_2 conversion rates and CH_4 selectivity all increase with the increase of ZrO_2 shell loading, and the three show a consistent changing trend. For all ZrO_2 shell loadings, the corresponding CO conversion rate is higher than the CO_2 conversion rate. When the ZrO_2 shell loading is 23%, m-SiO_2@ZrO_2-23% achieves relatively the best CO conversion rate, CO_2 conversion rate, and CH_4 selectivity, which are 13.07%, 10.33%, and 45.83%, respectively. Although the m-SiO_2@ZrO_2 core-shell support has catalytic performance, its catalytic effect is very poor, so reasonable design and modification must be carried out.

Characterization Analysis of Mesoporous SiO_2@ZrO_2 Core-Shell Support

Analyzing the structure and morphology of mesoporous SiO_2@ZrO_2 core-shell supports is the basis for regulating the performance of subsequent catalysts. The physicochemical properties of the supports are systematically characterized by means of XRD, SEM, TEM, BET, etc., to clarify the influence of the ZrO_2 shell on the support structure.

(1) XRD analysis of phase structure

Fig. 3 shows the XRD patterns of m-SiO_2@ZrO_2 and m-SiO_2@ZrO_2-t (t = 7%, 15%, 23%). It can be seen from the figure that SiO_2 exhibits a broad hump in the 2θ range of 15°~35° with a peak at 22.5°, indicating that the synthesized m-SiO_2 has an amorphous structure [17]. No other diffraction peaks are observed in the m-SiO_2@ZrO_2-t materials obtained after ZrO_2 shell loading, which may be due to the high dispersion of ZrO_2 on SiO_2 or the low loading amount of the ZrO_2 shell. With the increase of ZrO_2 shell loading, a broad hump is observed in all samples, indicating that the materials maintain the amorphous structure of SiO_2.

(2) SEM analysis of morphology distribution

Fig. 4 shows the SEM images of m-SiO_2 and m-SiO_2@ZrO_2-15% supports. Figs. 4a) and 4b) are SEM images of pure m-SiO_2, which present spherical particles with a diameter of approximately 100 nm. Fig. 4c) shows that after coating with a 15% ZrO_2 shell, the surface becomes slightly rough and the particles increase slightly, indicating that ZrO_2 is successfully coated

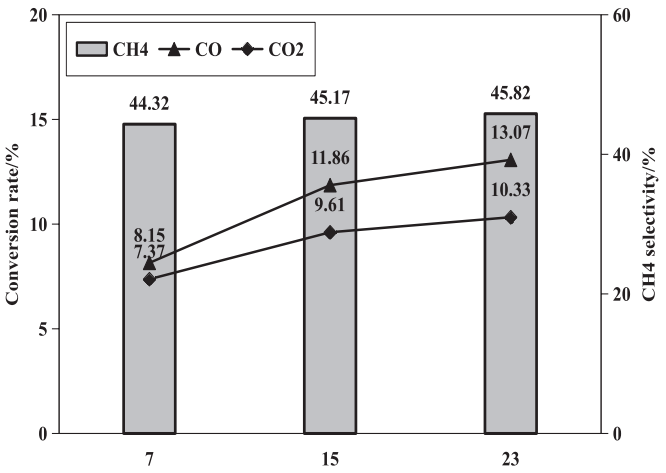

Fig. 2. Effects of different ZrO_2 shell loadings on CO/CO_2 conversion rates and CH_4 selectivity.

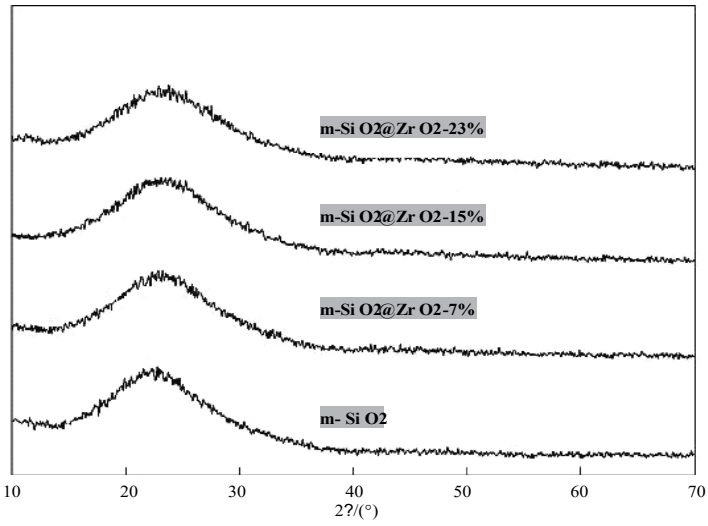

Fig. 3. XRD patterns of m-SiO_2@ZrO_2 and m-SiO_2@ZrO_2-t.

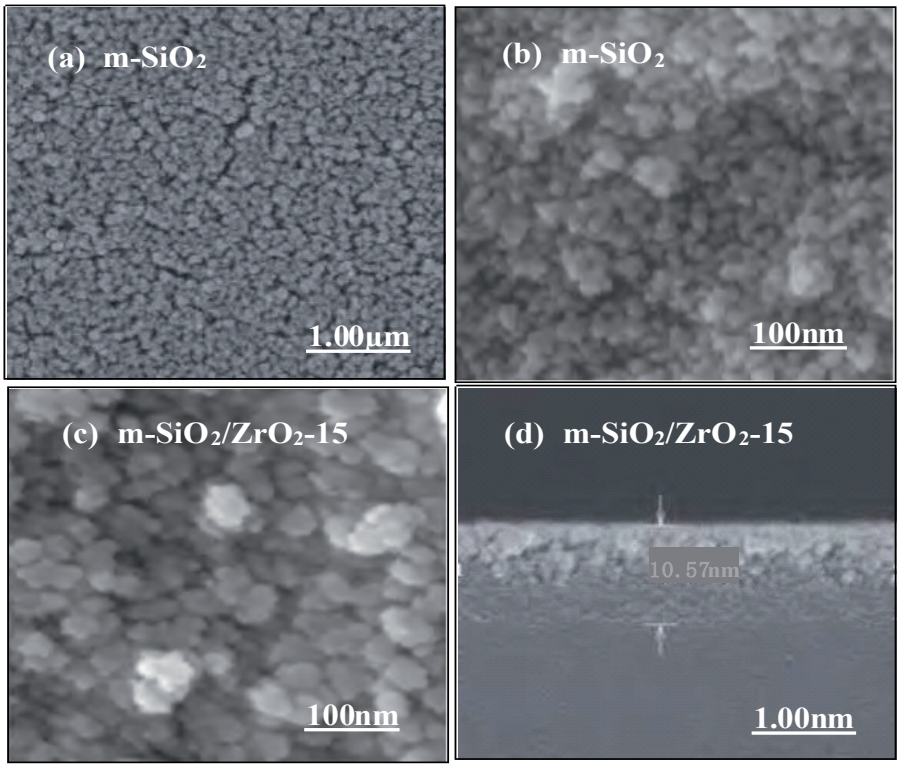

Fig. 4. SEM images of m-SiO_2@ZrO_2 and m-SiO_2@ZrO_2-15% supports.

without damaging the integrity of the SiO_2 core. It can be seen in Fig. 4d) that a ZrO_2 shell with a thickness of about 10.57 nm appears on the surface of m-SiO_2. SEM analysis reveals that a good m-SiO_2@ZrO_2 core-shell structured support is formed.

(3) BET analysis of pore structure and specific surface area

Table 1 shows the BET measurement results of m-SiO_2@ZrO_2 core-shell supports. The specific surface area (SSA) of m-SiO_2 is 926 m^2/g, the pore volume (Vp) is 1.29 cm^3/g, and the average pore diameter (Dp) is 6.2 nm. After coating with the ZrO_2 shell, the SSA and Vp decrease slightly. For example, the SSA of m-SiO_2@ZrO_2-15% is 704 m^2/g, and the Vp is 0.98 cm^3/g. This is due to ZrO_2 occupying part of the pore space, but the material still maintains high mesoporous characteristics (Dp = 4.5-5.7 nm). Moreover, with the increase of ZrO_2 shell loading, the pore size distribution gradually narrows. The pore size of m-SiO_2@ZrO_2-15% is concentrated around 4.9 nm, which is beneficial to

Table 1. BET measurement results of m-SiO_2@ZrO_2 core-shell supports.

	SSA (m^2/g)	Vp (cm^3/g)	Dp (nm)
m-SiO_2	926	1.29	6.2
m-SiO_2@ZrO_2-7%	782	1.08	5.7
m-SiO_2@ZrO_2-15%	704	0.98	4.9
m-SiO_2@ZrO_2-23%	639	0.87	4.5

the diffusion of reactants CO/CO_2. The core-shell structure successfully integrates the high specific surface area of SiO_2 and the surface activity of ZrO_2.

(4) XPS analysis of surface chemical properties of supports

Fig. 5 shows the XPS full spectrum and elemental spectra of the m-SiO_2@ZrO_2-15% core-shell support. It can be seen from Fig. 5d) that the sample contains three elements: Si, O, and Zr, indicating that ZrO_2 has been loaded onto SiO_2. In the high-resolution spectrum of Si, there is a Si 2p absorption peak at 103.4 eV, which is attributed to Si^{4+} in SiO_2. Compared with the binding energy of Si 2p in pure SiO_2 (103.7 eV), the value decreases by 0.3 eV, which is due to the electron transfer between SiO_2 and ZrO_2. As shown in Fig. 5c), the Zr 3d orbital is split into $3d_{5/2}$ (182.2 eV) and $3d_{3/2}$ (184.6 eV) with a binding energy difference of 2.4 eV, corresponding to the characteristic peak of Zr^{4+} [18], indicating that ZrO_2 exists in an oxidized state. From the fitting of the O 1s spectrum in Fig. 5a), lattice oxygen of Si–O (532.7 eV) and Zr–O (531.8 eV), as well as surface-adsorbed oxygen of –OH (533.5 eV), are obtained, which indicates that the support surface has abundant oxygen vacancies. This plays a positive role in the adsorption and activation of CO_2/CO. The research conclusions are as follows: The mesoporous SiO_2@ZrO_2 core-shell support is successfully prepared, with the optimal structure being a ZrO_2 shell loading of 15%. ZrO_2 is uniformly dispersed, the core-shell structure is intact, and the mesoporous characteristics are retained (SSA = 704 m^2/g, Dp = 4.9 nm), which is beneficial for mass transfer. The surface is rich in oxygen vacancies and Zr^{4+} active sites, which can enhance the interaction with metal components. This support provides an ideal "high dispersion + strong interaction" platform for the subsequent loading of Ni-CeO_2-ZnO and serves as the structural basis for improving the low-temperature activity and stability of the catalyst.

Ni-CeO_2-ZnO/m-SiO_2@ZrO_2 Catalyst Performance Evaluation and Characterization Analysis

Performance Evaluation and Characterization Analysis of Catalysts with Different Ni Loadings

Based on optimizing the mesoporous SiO_2@ZrO_2 core-shell support (with the optimal shell loading

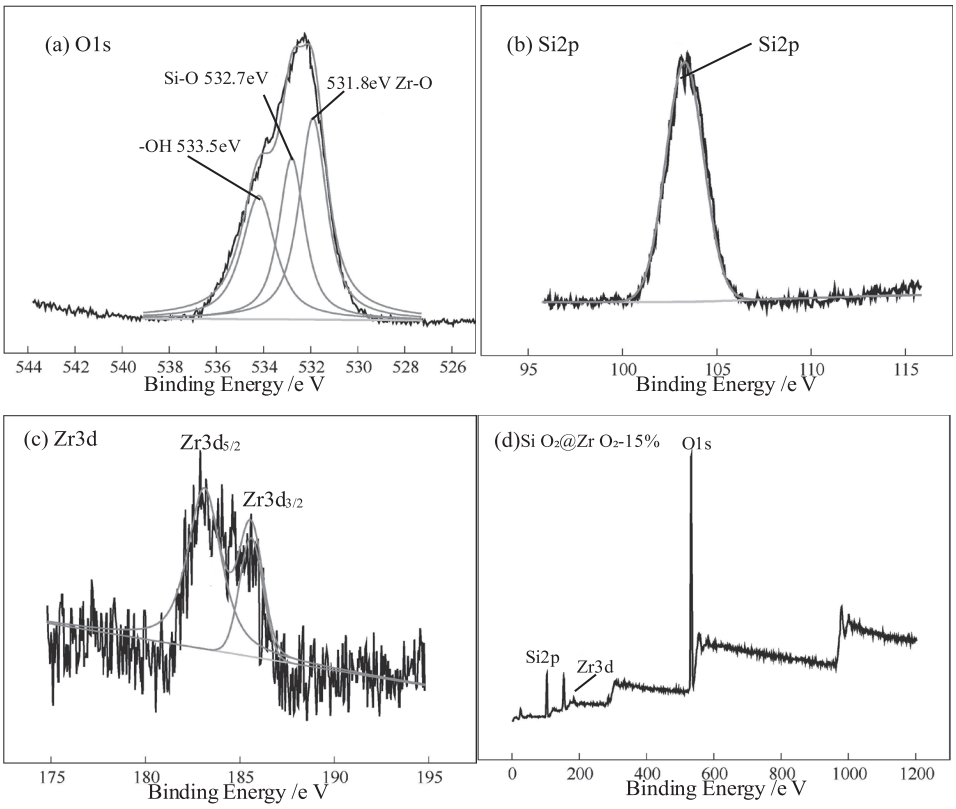

Fig. 5. XPS spectra of m-SiO_2@ZrO_2-15% core-shell support.

of 15%), the performance of Ni-CeO_2-ZnO/m-SiO_2@ZrO_2 catalysts prepared with different Ni loadings (5%, 10%, 15%, and 20%) was investigated with the Ce/Zn molar ratio fixed at 1:1 and the total promoter loading at 10%. Combined with activity evaluation and multi-dimensional characterization, the structure-activity relationship of the catalysts was clarified, and the optimal loading was screened out.

(1) Effect of Ni catalysts with different loadings on CO/CO_2 conversion rates and methane selectivity

Fig. 6 shows the effects of catalysts prepared with different Ni loadings (5%, 10%, 15%, and 20%) on CO/CO_2 conversion rates and methane selectivity at 250ºC and 300ºC, respectively, under the conditions of a fixed Ce/Zn molar ratio of 1:1 and a total promoter loading of 10%. It can be seen from Fig. 6 that in the low-temperature range of 250-300°C, the conversion rates of CO and CO_2 first increase and then decrease with the increase of Ni loading. When the loading is 10%, the conversion rates reach the maximum values: at 250ºC, the CO conversion rate reaches 78.5%, and the CO_2 conversion rate reaches 65.2%; at 300ºC, they rise to 92.3% and 87.6%, respectively, and the CH_4 selectivity basically remains above 99%.

(2) Characterization analysis of Ni-loaded catalysts

Fig. 7 shows the XRD patterns of catalyst samples after hydrogen reduction. In the XRD patterns, diffraction peaks of SiO_2 and ZrO_2 are observed, along with diffraction peaks of Ce-Zn-O alloy. Additionally, all catalysts exhibit diffraction peaks corresponding to the (111) and (200) crystal planes of face-centered cubic Ni at 44.5° and 51.9°, respectively. The intensity of the Ni diffraction peaks increases with the increase of Ni loading, which also indicates that the particle size is increasing.

Fig. 8a) shows the TEM image of the catalyst with 10% Ni loading, where the particles are distributed relatively uniformly. The inset in the figure presents

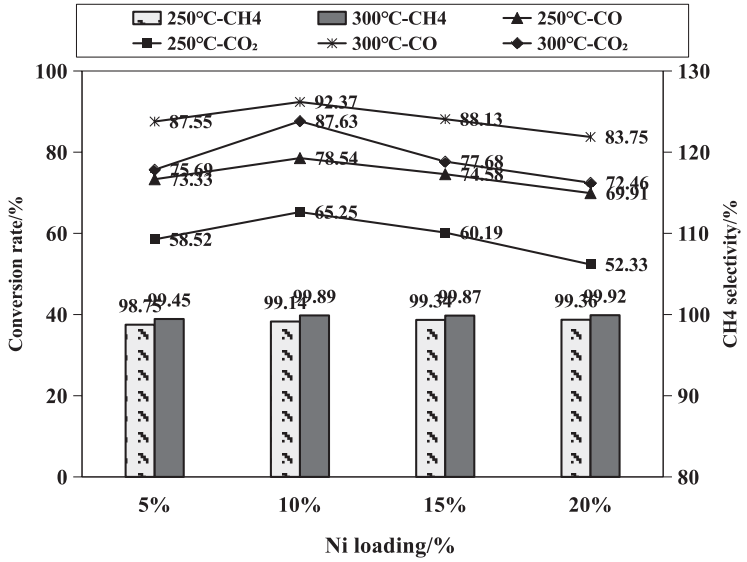

Fig. 6. Effect of Ni catalysts with different loadings on CO/CO_2 conversion rates and methane selectivity.

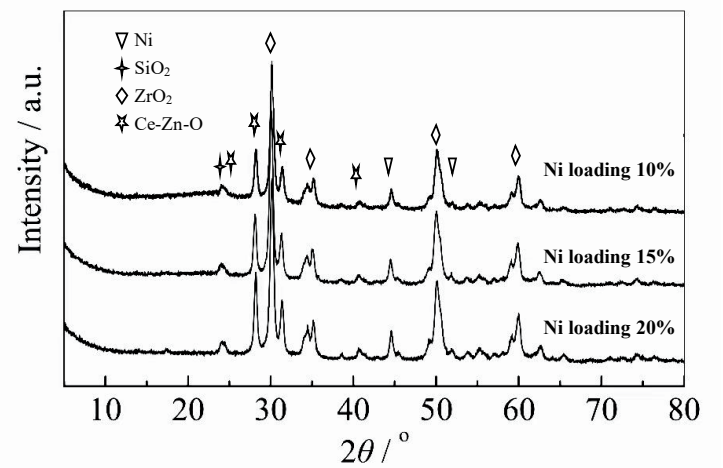

Fig. 7. XRD patterns of Ni catalysts with different loadings.

a local TEM image of a typical particle, from which it can be seen that Ni nanoparticles are uniformly dispersed on the support. Fig. 8b) is the TEM image of the catalyst after ZrO_2 coating, which exhibits obvious core-shell structural characteristics, with several agglomerated SiO_2 particles encapsulated within the ZrO_2 shell. Abundant pore structures can also be observed in Fig. 8b), which once again confirms that the catalyst has a large specific surface area, which is beneficial for the adsorption and activation of reaction molecules. In addition, the porosity is conducive to the migration of molecules to the surface of inner-layer particles. These two factors contribute to the improvement of catalyst activity.

Fig. 9 shows the H_2-TPR profile of the catalyst with 10% Ni loading. For NiO that is not loaded on the support or has no interaction with the support-promoter, the reduction peak of Ni species usually appears between 350-400ºC; when NiO is loaded on the support and has a strong interaction with the support-promoter, the corresponding reduction peak of Ni species will appear after 500°C, and the dispersion of the corresponding Ni species is also higher [19]. It can be seen from Fig. 9 that the catalyst exhibits a hydrogen reduction peak at around 350ºC, indicating that part of the Ni species in the catalyst exists in a form similar to pure NiO. The catalyst also has a hydrogen reduction peak at around 525ºC, indicating that another part of the Ni species has a strong interaction with the support-promoter. This is mainly due to the formation of Ce–O–Zn bonds, Zr–O–Si bonds, etc. in the composite, which leads to a strong interaction between Ni species and the support, promotes the dispersion of Ni species on the support surface [20], and can inhibit particle sintering during the catalytic process.

Table 2 presents the BET measurement results of catalysts with different Ni loadings. It can be seen from the table that the specific surface area (SSA), pore volume (Vp), and average pore size (Dp) decrease with the increase of Ni loading. Combined with the influence of loading on conversion rates and selectivity, the 10% Ni loading shows the best performance, with a specific

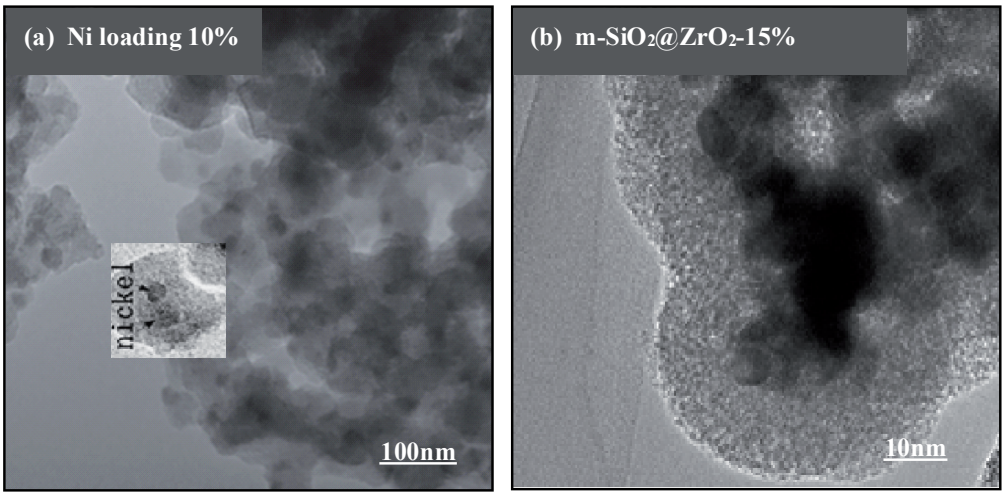

Fig. 8. TEM images of the catalyst with 10% Ni loading and m-SiO_2@ZrO_2-15% support.

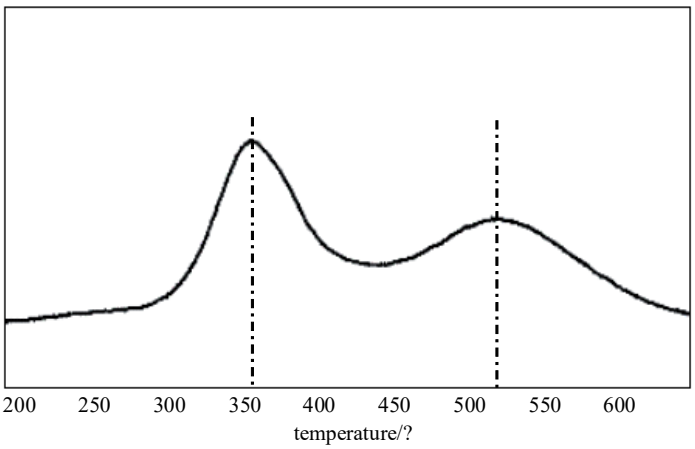

Fig. 9. H_2-TPR profile of the catalyst with 10% Ni loading.

Table 2. BET measurement results of catalysts with different Ni loadings.

Ni loading (%)	SSA (m^2/g)	Vp (cm^3/g)	Dp (nm)
5	661	0.89	4.6
10	616	0.85	4.4
15	537	0.73	3.9
20	411	0.60	3.5

surface area of 586 m^2/g and a pore volume of 0.82 cm^3/g, still maintaining a good mesoporous structure. However, when the Ni loading reaches 20%, the pores are blocked, the specific surface area drops to 411 m^2/g, and the blocked pores lead to increased mass transfer resistance.

Performance Evaluation and Characterization Analysis of Catalysts with Different Ce/Zn Molar Ratios

Based on optimizing the mesoporous SiO_2@ZrO_2 core-shell support (with the optimal shell loading of 15%), the performance of Ni-CeO_2-ZnO/m-SiO_2@ZrO_2 catalysts prepared with different Ce/Zn molar ratios (3:1, 1:1, 1:3) was investigated under the conditions of fixing the total Ce/Zn loading at 10% and the Ni loading at 10%. Combined with activity evaluation and multi-dimensional characterization, the structure-activity relationship of the catalysts was clarified, and the optimal Ce/Zn molar ratio was screened out.

(1) Effect of catalysts with different Ce/Zn molar ratios on CO/CO_2 conversion rates and methane selectivity

Fig. 10 shows the effect of catalysts prepared by adjusting the Ce/Zn molar ratio (3:1, 1:1, 1:3) with a fixed Ni loading of 10% on CO/CO_2 conversion rates and methane selectivity. The results indicate that the catalyst exhibits optimal performance when the Ce/Zn molar ratio is 1:1 at 300ºC, the CO conversion rate reaches 92.3%, and the CO_2 conversion rate reaches 87.6%, with no significant difference in the CH_4 selectivity (all>99%).

(2) Characterization analysis of catalysts with different Ce/Zn molar ratios

As can be seen from Fig. 11, when the Ce/Zn molar ratio is 3:1, agglomeration occurs, which may be the agglomeration of CeO_2, and this is not conducive to the dispersion of active metal nickel. When the Ce/Zn molar ratio is 1:3, the phenomenon that Ni active sites are covered is observed, which may be caused by the coverage of ZnO. Both of these ratios weaken the synergistic effect and cannot fully exert the catalytic effect. When the Ce/Zn molar ratio is 1:1, the Ni particles are evenly dispersed, and a "Ni-CeO_2-ZnO" ternary interface is formed around them, thus achieving a better catalytic effect.

Table 3 presents the BET measurement results of catalysts with different Ce/Zn molar ratios. It can be seen from the table that when the Ce/Zn molar ratios are 3:1 and 1:3, the specific surface area (SSA), pore volume (Vp), and average pore size (Dp) are all relatively smaller compared to the catalyst with a Ce/Zn molar ratio of 1:1. This is mainly due to agglomeration or coverage, which causes blockage of the catalyst pores. The measurement results are also consistent with the TEM findings.

Structural Summary of the Optimal Catalyst

From the comprehensive analysis, it is determined that the optimal catalyst is Ni_{10}-$Ce_{0.5}Zn_{0.5}O$/m-SiO_2@ZrO_2-15%, and its structure and performance are summarized as follows: The 15% ZrO_2-loaded shell uniformly coats the SiO_2 core; H_2-TPR indicates a strong metal-support interaction, which collectively ensures the

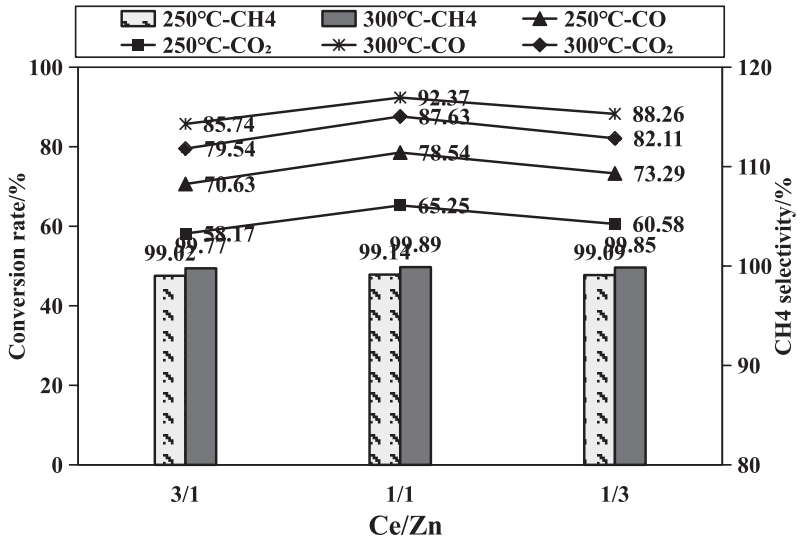

Fig. 10. Effect of catalysts with different Ce/Zn molar ratios on CO/CO_2 conversion rates and methane selectivity.

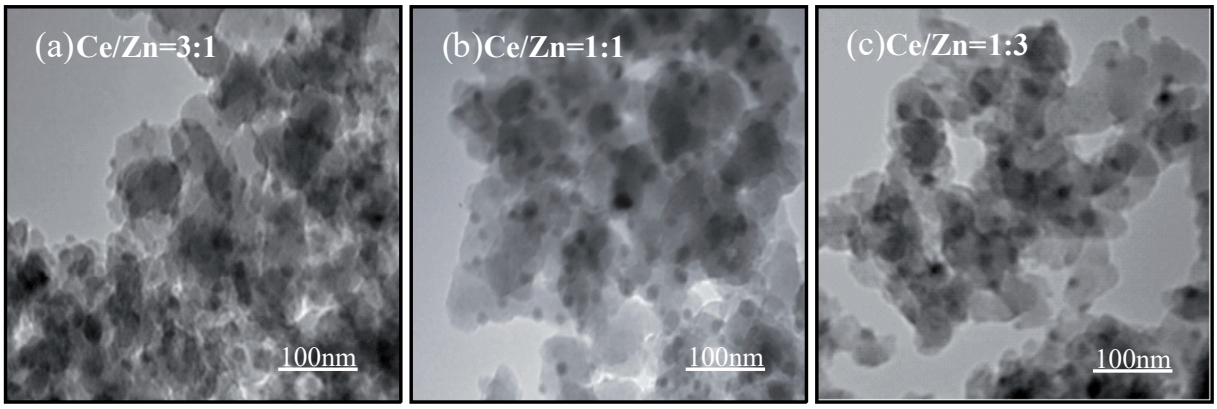

Fig. 11. TEM images of catalysts with different Ce/Zn molar ratios.

Table 3. BET measurement results of catalysts with different Ce/Zn molar ratios.

Ce/Zn	SSA (m^2/g)	Vp (cm^3/g)	Dp (nm)
3:1	587	0.81	4.3
1:1	616	0.85	4.4
1:3	555	0.78	4.1

stability of active sites; the mesoporous characteristics in the pore structure are retained, ensuring the rapid diffusion of reactants to the active sites.

The optimal preparation parameters of the catalyst are a Ni loading of 10% and a Ce/Zn molar ratio of 1:1. The interaction between the active component Ni and the support/promoter is moderate, maximizing the number of active sites; CeO_2-ZnO synergistically regulates the electronic properties and oxygen vacancies (Ce^{3+}/Ce^{4+} cycle), enhancing the activation of CO/CO_2 and the conversion of intermediate products; the mesoporous structure is not destroyed, resulting in low mass transfer resistance, which is suitable for the rapid conversion of high-concentration components in coal pyrolysis gas.

Evaluation of Sulfur Poisoning Resistance, Sintering Resistance, and Stability of the Catalyst

Trace amounts of H_2S (50-500 ppm) in coal pyrolysis gas and high-temperature reaction conditions can easily cause catalyst sulfur poisoning, metal sintering, and carbon deposition deactivation. Therefore, this section focuses on evaluating the sulfur resistance, sintering resistance, and long-term stability of the optimal catalyst (Ni_{10}-$Ce_{0.5}Zn_{0.5}O$/m-SiO_2@ZrO_2-15%), and reveals its action mechanism through characterization.

Evaluation of Stability and Sulfur Poisoning Resistance

Fig. 12 shows the CO/CO_2 conversion rates of the optimal catalyst during 500 h of continuous operation at 300ºC in simulated coal pyrolysis gas with the introduction of 50 ppm H_2S. The results

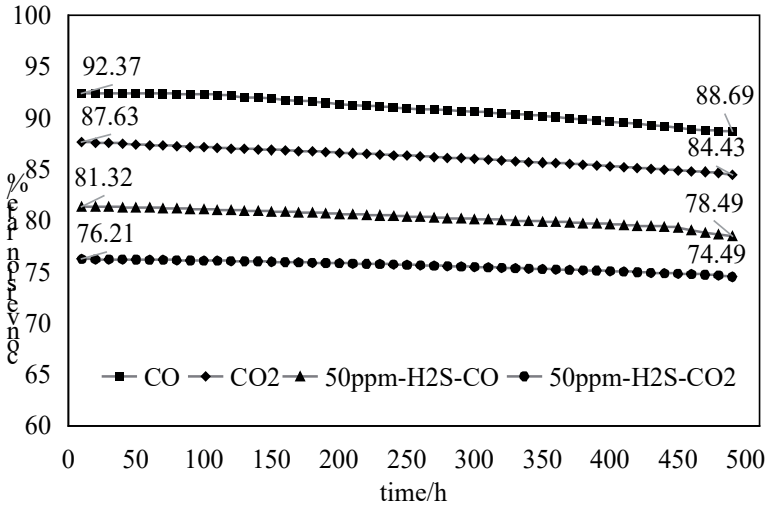

Fig. 12. Evaluation of stability and sulfur resistance of the optimal catalyst.

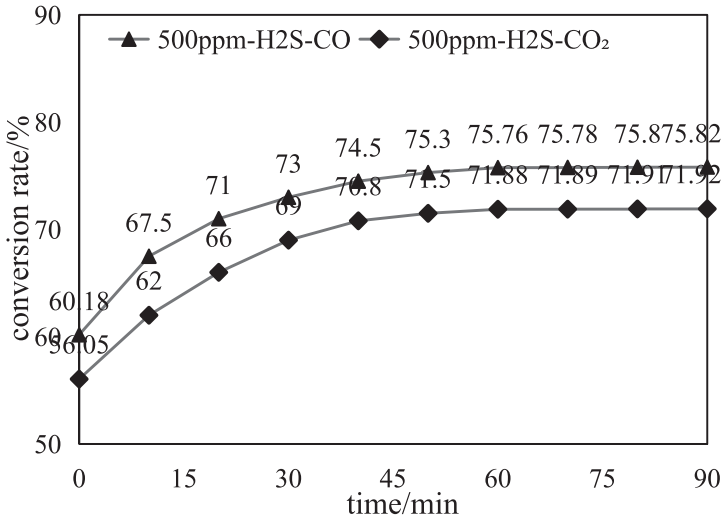

Fig. 13. Activity evaluation of the optimal catalyst in an environment containing 500 ppm H_2S.

indicate that under sulfur-free conditions, after 500 h of continuous operation at 300ºC, the CO and CO_2 conversion rates of the optimal catalyst are 88.69% and 78.49%, respectively, maintaining high efficiency with minimal decay. After introducing 50 ppm H_2S, the initial CO conversion rate decreases from 92.37% to 81.32%, and the initial CO_2 conversion rate drops from 87.63% to 76.21%, suggesting that the initial activity of the optimal catalyst decreases by approximately 12%, but remains stable in the subsequent 500 h. It can be concluded that the optimal catalyst exhibits high stability and sulfur resistance. As can be seen from Fig. 12, the change curves of CO and CO_2 conversion rates over time do not show abrupt changes, which also proves that the optimal catalyst has anti-coking performance. The main mechanism is that the Ce^{3+}/Ce^{4+} redox cycle of CeO_2 provides lattice oxygen (O*), which oxidizes the deposited carbon into CO/CO_2, while the electronic effect of ZnO inhibits the dissociation of CO/CO_2 to form carbon species, and the two synergistically reduce coke formation. Meanwhile, at 300°C, the strong metal-support interaction of the ZrO_2 shell stabilizes the valence state of Ni and inhibits its migration and agglomeration [21], demonstrating its anti-sintering performance.

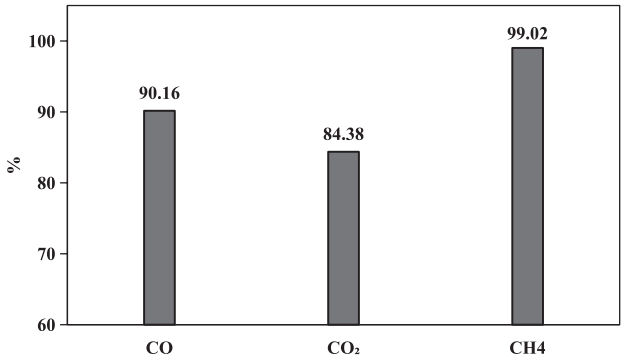

Fig. 14. Effect of the optimal catalyst on CO/CO_2 conversion rates and methane selectivity in real coal pyrolysis gas.

Fig. 13 shows the CO and CO_2 conversion rates of the optimal catalyst after introducing 500 ppm H_2S during operation at 300ºC in simulated pyrolysis gas until stabilization, followed by stopping the introduction of H_2S. It can be seen from Fig. 13 that in the environment with 500 ppm H_2S, the CO and CO_2 conversion rates drop to 60.18% and 56.05%, respectively, and the activity of the optimal catalyst decreases by approximately 35%, but it is still higher than the activity of traditional catalysts under the same conditions. After stopping the introduction of H_2S, the CO and CO_2 conversion rates increase to 75.76% and 71.88%, respectively, after 60 min, and then tend to be stable. The catalyst activity can be restored to about 82% of the initial value, indicating that the sulfur poisoning of the optimal catalyst has partial reversibility. The reason for the sulfur resistance is mainly that ZnO preferentially reacts with H_2S to form ZnS, reducing the occupation of Ni active sites by sulfur [22].

Verification with Real Coal Pyrolysis Gas

The real coal pyrolysis gas, after pretreatment to remove tar, has a gas composition of 28% CO, 17% CO_2, 51% H_2, 80 ppm H_2S, and approximately 4% other gases. A sufficient amount of H_2 was introduced, and the catalytic reaction was carried out at 300°C. After stabilization, the CO and CO_2 conversion rates and methane selectivity were detected and calculated, with the results shown in Fig. 14. The results indicate that the CO and CO_2 conversion rates reach 90.16% and 84.34%, respectively, and the CH_4 selectivity is 99.02%, confirming the adaptability of the optimal catalyst to real complex gas sources.

Conclusions

This study addresses low-temperature CO/CO_2 methanation bottlenecks in coal pyrolysis gas via an innovative composite catalyst design, highlighting its novelties, key findings, and practical value. The main points are as follows:

(1) The catalyst features synergistic regulation of a mesoporous $SiO_2@ZrO_2$ core-shell support, Ni active sites, and CeO_2–ZnO promoters; we optimized the support structure and preparation parameters, and investigated its catalytic performance, sulfur resistance, and stability.

(2) The optimal $SiO_2@ZrO_2$ support (15% ZrO_2 shell loading) integrates SiO_2's high specific surface area with ZrO_2's oxygen vacancies to stabilize active components.

(3) The best catalyst (10% Ni loading, Ce/Zn = 1:1) achieves 92.37% CO conversion, 87.63% CO_2 conversion, and >99% CH_4 selectivity at 300ºC, via CeO_2-ZnO synergy (oxygen vacancies for activation, Ni enhancement, and poisoning suppression).

(4) It has excellent stability: ZnO protects Ni from H_2S (partially reversible poisoning), and CeO_2 oxidizes coke; the core innovation (synergistic support-promoter regulation) enables simultaneous high activity, stability, and anti-toxicity, providing a practical methanation strategy.

Acknowledgments

This work was financially supported by the Xinjiang Industry and Information Technology Sector Key Industries Talent Support Program (No. XJRC-2025-GX-ZDCY-04) and the Xinjiang Uygur Autonomous Region Natural Science Foundation (Youth Fund, Southern Xinjiang United Fund) (No. 20261153358).

Conflict of Interest

The authors declare no conflict of interest.

References

1. LI S., SHEN Q., SONG X., YU W., SUN N., WEI W. Impacts Analysis of Dual Carbon Target on the Medium- and Long-Term Petroleum Products Demand in China. Energies, **16** (8), 3584, **2023**.
2. LIU J., ZHUANG C., DU W.J. Life Cycle Assessment of the Coal-to-Synthetic Natural Gas/Methanol Coproduction Process in Series. ACS Sustainable Chemistry & Engineering, **12** (35), 13297, **2024**.
3. PANGESTU M.R.G., MALAIBARI Z., MUHAMMAD A., AL-ROWAILI F.N., ZAHID U. Comprehensive Review on Methane Pyrolysis for Sustainable Hydrogen Production. Energy & Fuels, **38** (15), 13514, **2024**.
4. PENG T., ZHOU N., ZHANG C., YANG X., MENG X., DAI Z., XIONG Y. Metalloporphyrin- and Phosphonium-Bifunctionalized Porous Organic Polymers for Efficient Synergistic Catalysis of CO_2 Conversion under Mild Conditions. ACS Applied Materials & Interfaces, **16** (48), 66032, **2024**.
5. ZHAO Y., KANG Y., LI H., LI H. CO_2 Conversion to Synthesis Gas via DRM on the Durable Al_2O_3/Ni/Al_2O_3 Sandwich Catalyst with High Activity and Stability. Green Chemistry, **20** (11), 2781, **2018**.
6. WU J., CHEN J., DING Z.B., YANG H., WANG X., RUI Z. Strategies for Improving Sulfur Resistance of Lean Methane Oxidation Catalysts: Progresses and Future Perspectives. Chemical Engineering Journal, **479**, 147640, **2024**.
7. YUAN B., ZHU T., HAN Y., ZHANG X., WANG M., LI C. Deactivation Mechanism and Anti-Deactivation Measures of Metal Catalyst in the Dry Reforming of Methane: A Review. Atmosphere, **14** (5), 770, **2023**.
8. XU Q., ZHENG Z., LUO J., LAI Z., CHEN J., SHANG J. Efficient MnFe/Al_2O_3 Catalyst for NH_3-SCR of NO at Low Temperature: The Influence of Strong Interactions between Active Components and the Carrier. Catalysis Science & Technology, **14** (10), 2929, **2024**.
9. HU Y., MEN Y., XU S., FENG Y., WANG J., LIU K., ZHANG Y. Modulating Nickel Precursors to Construct Highly Active Ni/Y_2O_3 Catalysts for CO_2 Methanation. International Journal of Hydrogen Energy, **81**, 1311, **2024**.
10. YANG L., YOU X., SHENG Z., MA D., YU D., XIAO X., WANG S. The Promoting Effect of Noble Metal (Rh, Ru, Pt, Pd) Doping on the Performances of MnO_x-CeO_2/Graphene Catalysts for the Selective Catalytic Reduction of NO with NH_3 at Low Temperatures. New Journal of Chemistry, **42** (14), 11673,**2018**.
11. SONG K.H., JEONG S.K., JEONG B.H., LEE K.Y., KIM H.J. Effect of the Ni/Al Ratio on the Performance of $NiAl_2O_4$ Spinel-Based Catalysts for Supercritical Methylcyclohexane Catalytic Cracking. Catalysts, **11** (3), 323, **2021**.
12. WANG C., JIANG C., BAI J., YANG G., WU R., ZHAO Y., XIAO T. Effect of Pore Structures on 1,4-Butynediol Hydrogenation over Mesoporous Ni/Al_2O_3-SiO_2 Catalysts. Industrial & Engineering Chemistry Research, **60** (49), 17840,**2021**.
13. CHEN Y., SUN L., LI Y., CAO Y., GUAN W., PAN J., ZHANG Z., ZHANG Y. Oxygen Vacancy-Induced Metal-Support Interactions in AuPd/ZrO_2 Catalysts for Boosting 5-Hydroxymethylfurfural Oxidation. Inorganic Chemistry, 62 (37), 15277, **2023**.
14. PEERA S.G., KIM S.W. Rare Earth Ce/CeO_2 Electrocatalysts: Role of High Electronic Spin State of Ce and Ce^{3+}/Ce^{4+} Redox Couple on Oxygen Reduction Reaction. Nanomaterials, **15** (8), 600, **2025**.
15. ZHANG W., LIU T., TAN Q., LI J., MA Y., HE Y., HAN D., QIN D., NIU L. Atomically Precise Dinuclear Ni Active Site-Modified MOF-Derived ZnO@NC Heterojunction toward High-Performance N_2 Photofixation. ACS Catalysis, **13** (5), 3242, **2023**.
16. CUI S., WANG Z., ZHAO H., SUN H., WEI Q., WANG L. Core-Shell Ni/$SiO_2@ZrO_2$ Catalyst for Highly Selective CO_2 Conversion Accompanied by Enhancing Reaction Stability. Heliyon, **10** (23), e40697, **2024**.
17. FU L., WANG Y., RIEKEHR L., RÄTHEL J., ENGQVIST H., XIA W. Observation of Yttrium Oxide Segregation in a ZrO_2-SiO_2 Glass-Ceramic at Nanometer Dimensions. Journal of the Ceramic Society of Japan, 103 (12), 7147, **2020**.

18. LAM E., LARMIER K., TADA S., WOLF P., SAFONOVA O.V., COPÉRET C. Zr(IV) Surface Sites Determine CH_3OH Formation Rate on $Cu/ZrO_2/SiO_2$-CO_2 Hydrogenation Catalysts. Chinese Journal of Catalysis, **40** (11), 1741, **2019**.
19. SUN X., WU B., LI B., ZHAO J., LI S., ZHENG M., CHEN J., ZHANG H. Strong Metal-Support Interactions for High Sintering Resistance of Ru-Based Catalysts toward the HER and ORR. Chemical Communications, **59** (68), 10291, **2023**.
20. LI S., WANG X., CAO M., LU J., QIU L., YAN X. Engineering the Interface and Interaction Structure on Highly Coke-Resistant Ni/CeO_2-Al_2O_3 Catalyst for Dry Reforming of Methane. Chinese Journal of Structural Chemistry, **41** (12), 7, **2022**.
21. ZHAO L., ZHAO J., WU T., ZHAO M., YAN W., ZHANG Y., LI H., WANG Y., XIAO T., ZHAO Y. Synergistic Effect of Oxygen Vacancies and Ni Species on Tuning Selectivity of Ni/ZrO_2 Catalyst for Hydrogenation of Maleic Anhydride into Succinic Anhydride and γ-Butyrolacetone. Nanomaterials, **9** (3), 406, **2019**.
22. CHEN J.H., XIA F., LI Y., LI J., TONG M. Study on the Preparation of Hydrogen-Rich Fuel Gas from Mixed Pyrolysis of Coal by Alkaline Earth Metal Oxide Supported γ-Al_2O_3 Catalyst. Polish Journal of Environmental Studies, **31** (4), 3121, **2022**.